

# Finite element analysis of reinforced concrete beams with UHPFRC retrofitting

Hokkaido University  
Hokkaido University  
Civil Engineering Research Institute for Cold Region

Student member ○Muhammad Safdar  
Member Takashi Matsumoto  
Member Ko Kakuma

## 1. INTRODUCTION

Under normal circumstances, reinforced concrete structures show excellent performance in terms of structural behavior and durability except for the zones that are subjected to severe environmental conditions and high mechanical loading<sup>1)</sup>. The rehabilitation of deteriorated concrete structures is a major problem from a sustainability point of view. Sustainable infrastructures require the use of new high-tech materials such as high-performance concrete (HPC) and ultra-high performance fiber reinforced concrete (UHPFRC) in order to minimize the intervention during the life span. Increasing requirements of load bearing capacity, durability and safety concern of concrete structures also demand the UHPFRC for repair and maintenance.

In general, UHPFRC can be described as a composite material comprised of fine sand, a high amount of silica fume, cement, water, superplasticizer, low water-binder ratio, relatively large proportion of short steel fibers, thus, making the composite with superior characteristics such as self-compacting, very high strength, high modulus of elasticity and extremely low permeability that prevents the ingress of detrimental substances such as water and chloride ion<sup>2)</sup>. Typical strengths are of 150 to 200MPa and 7 to 11MPa in compression and uniaxial tension respectively<sup>2)</sup>. Moreover, this material exhibits outstanding tensile behavior, characterized by four domains<sup>3)</sup>. In the first domain, there is a linear-elastic stress rise without crack formation. The second domain is described by strain hardening with the formation of distributed micro-cracks of small width (<50 μm), until localized macro-cracks form at maximum stress and propagate in the third domain. Finally, no more stress is transferred through these localized macro-cracks at final fracture. Because of these properties, UHPFRC has an increased resistance against environmental degradation of concrete and high mechanical loading. Thus, UHPFRC is a promising material to significantly improve structural resistance and durability of deteriorated concrete structures.

The present study demonstrates the flexural behavior of reinforced concrete beams retrofitted with UHPFRC by comparing experimental results with 3-D finite element analysis. The experimental and analytical results disclose that the ultimate strength and stiffness of reinforced concrete beams, which were repaired in the tension zone, are increased with the increase of UHPFRC thickness.

## 2. EXPERIMENTAL BEAM DESCRIPTION

The study was carried out by performing four-point bending tests on beams at different cross-sectional repair positions by the incorporation of UHPFRC under optimized laboratory conditions. **Table 1** lists the experimental details after repairing of upper and lower cross-sectional positions with UHPFRC of varying thicknesses. **Fig. 1(a)** shows the proposed geometry of reference beam (B-0) for the experiment without the incorporation of UHPFRC. The length and span of these beams are 3000 mm and 2800 mm respectively. The shear span ratio of the beams is 2.8 and D10 stirrups are provided at 200 mm intervals. **Fig. 1(b)** shows the cross-section of seven different specimens, with the width and height are 250 mm and 400 mm respectively.

**Table 1** Experimental beam description

Specimen	Repair location	Repair thickness (mm)
B-0	No repair	-
BU-20	Upper	20
BU-40		40
BU-60		60
BL-20	Lower	20
BL-40		40
BL-60		60

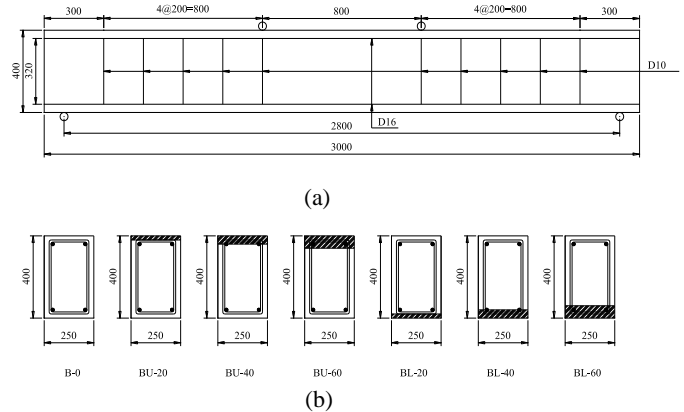


**Fig. 1** (a) Reference beam (B-0) geometry (b) Beam cross sections with different repair thickness

Two D16 bars are provided both in tension and compression zone of the beam. The beam is designed as flexural failure type with the tolerance of 3.1.

## 3. ANALYTICAL MODEL

Finite element analysis is performed by using a nonlinear FEM software i.e. Marc/Mentat. The quarter models are adopted, because specimen load conditions are symmetric as shown in **Fig. 2(a)**. As for the element, 8-nodes 3D solid elements are used for concrete and UHPFRC. The steel reinforcement is idealized using rod/truss element with the node points defined each rebar element sharing common nodes with the concrete solids. This approach is called discrete idealization of rebar with the concrete. The reinforcement layout for quarter symmetric beam and bar area is given in **Fig. 2(b)**. The nonlinear material properties of steel are entered using von Mises yield criteria. The non-linear concrete cracking formulation used by MSC/Marc is called "Buyukozturk" model and defined by equation (1).

$$f = \beta\sqrt{3}\bar{\sigma}J_1 + \gamma J_1^2 + 3J_2 - \bar{\sigma}^2 \quad (1)$$

Where  $\beta$  and  $\gamma$  are 1.732, 0.2 respectively.  $\bar{\sigma}$  is equivalent stress; equal to one-third of uniaxial compressive stress,  $J_1$  and  $J_2$  are stress invariants<sup>4)</sup>. The model is divided into a total 2400 elements for concrete and the meshing in UHPFRC layer finer than normal concrete. Loading is given by load increment of displacement control with 0.0075mm/increment. The bond between reinforcing bar and concrete is assumed perfect. The boundary conditions for quarter symmetric beam are shown in **Fig. 2(c)**.

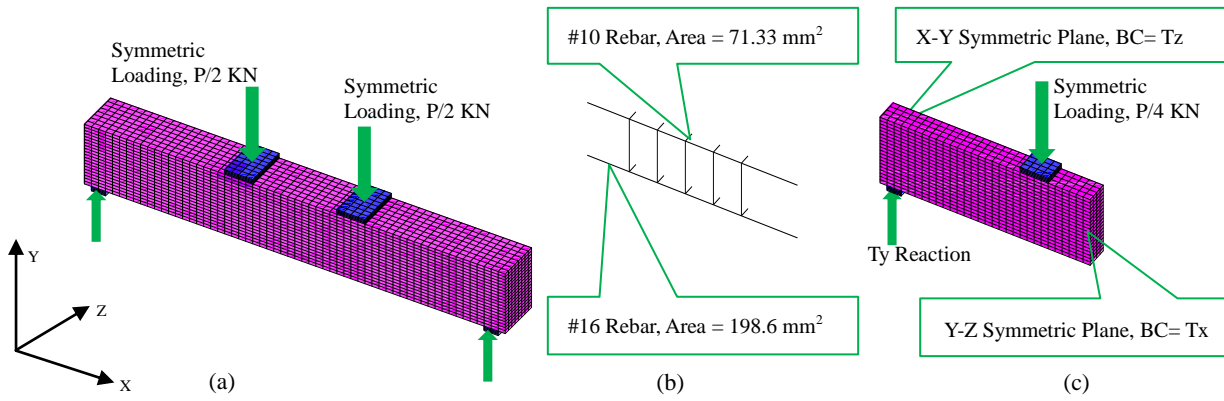


Fig. 2 (a) Full RC model, (b) Reinforcement layout, (c) Boundary conditions

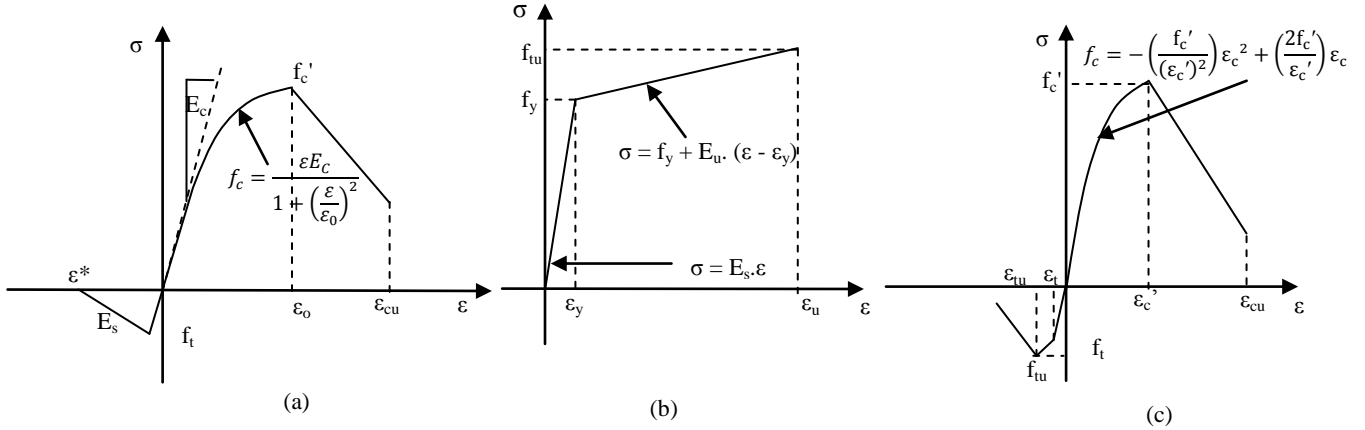


Fig. 3 Stress-strain curves for, (a) Concrete, (b) Steel, (c) UHPFRC

#### 4. MODELING OF MATERIAL BEHAVIOURS

##### 4.1 Concrete

In this study, the concrete is assumed homogenous and initially isotropic. The uniaxial compressive stress-strain relationship for the concrete model as shown in Fig. 3(a). In the compression zone, linear elasticity is used when  $0 \leq \sigma \leq 0.3f'_c$ , MacGergor 1992 equation is used when  $0.3f'_c \leq \sigma \leq f'_c$ , and a linear softening elastoplasticity model until a specified ultimate strain is reached. The ultimate strain of concrete design is used with around 0.003. However, it is said that the ultimate strain when a reinforced concrete beam failures by bending reaches about 2 times of strain when concrete by a compression test failures, therefore,  $\epsilon_{cu} = 0.006$  is adopted<sup>5)</sup>. In tension zone, linear elasticity is used before cracking, i.e. until tension strength of concrete reaches  $f_t$  i.e. 2.235MPa, a linear softening elastoplasticity model after cracking, i.e.  $f_t$  and equal to one-tenth of young's modulus, i.e. 2430MPa.

##### 4.2 Steel

Fig. 3(b) shows the constitutive law of reinforcing bar. In this analysis, linear elasticity is used when  $0 \leq \sigma \leq f_y$  and a linear hardening elastoplasticity model until a specified ultimate strain is reached in tension and compression. The yield strength  $f_y$  and ultimate strength  $f_{tu}$  of reinforcing bar SD345-D16 are provided with 386MPa and 546MPa respectively. The ultimate strain  $\epsilon_u$  used in this study is 0.24. As for SD345-D10 reinforcement, the yield strength  $f_y$  and ultimate strain  $\epsilon_u$  are 376MPa and 0.28 respectively. Poisson's ratio of 0.3 is used for the reinforcing bars in this study. The elastic modulus  $E_s$  of both steels is assumed 200GPa.

##### 4.3 UHPFRC

Fig. 3(c) shows the uniaxial compressive stress-strain relationship for the UHPFRC model which is obtained by using a parabolic equation before maximum strength  $f'_c$ . A linear

softening elastoplasticity model is used once the maximum compressive strength is reached. The 42 days uniaxial compressive strength  $f'_c$  and initial modulus of elasticity  $E_c$  of UHPFRC are 156.3MPa and 34600MPa respectively. Poisson's ratio of 0.2 is used for UHPFRC in this study. In tension zone, a bilinear relation is idealized using the average tensile properties obtained by tension test followed by the softening after reaching  $f_{tu}$  is used. The crack starts developing in UHPFRC when the stress reaches the cracking stress  $f_t$ , followed by strain hardening until ultimate strength  $f_{tu}$ , then localized cracking takes place. The cracking strength  $f_t$  and ultimate tensile strength  $f_{tu}$  are provided with 7.4MPa and 10.1MPa, respectively, obtained by experiments. The average maximum tensile deformation in the strain-hardening domain is of 4800 $\mu$ . It means small crack distribution is wide (strain hardening zone).

#### 5. RESULTS AND DISCUSSIONS

##### 5.1 Load Deflection Curves

In Fig. 4, the relationship between load and deflection of center span is shown along with ACI deflection, ultimate load and crack initiation. Three stages (a) linear elastic-uncracked, (b) elastic-cracked, (c) ultimate stage can be distinguished in the curves. In general, the load-deflection curves for the beams from the analytical analysis are not in close agreement with the experimental results. In linear elastic-uncracked stage, the analytical load-deflection curves are slightly stiffer than the experimental curves. After the linear elastic-uncracked stage, the stiffness of the finite element model is again higher than of the experimental beams. As for this, many effects cause higher stiffness in the analytical model. First, dry shrinkage, heat evaluation during hydration and handling of beams cause the micro-cracks in the concrete for experimental beams while the analytical models do not include the micro-cracks. Due to these effects, the stiffness of experimental beams reduces due to the

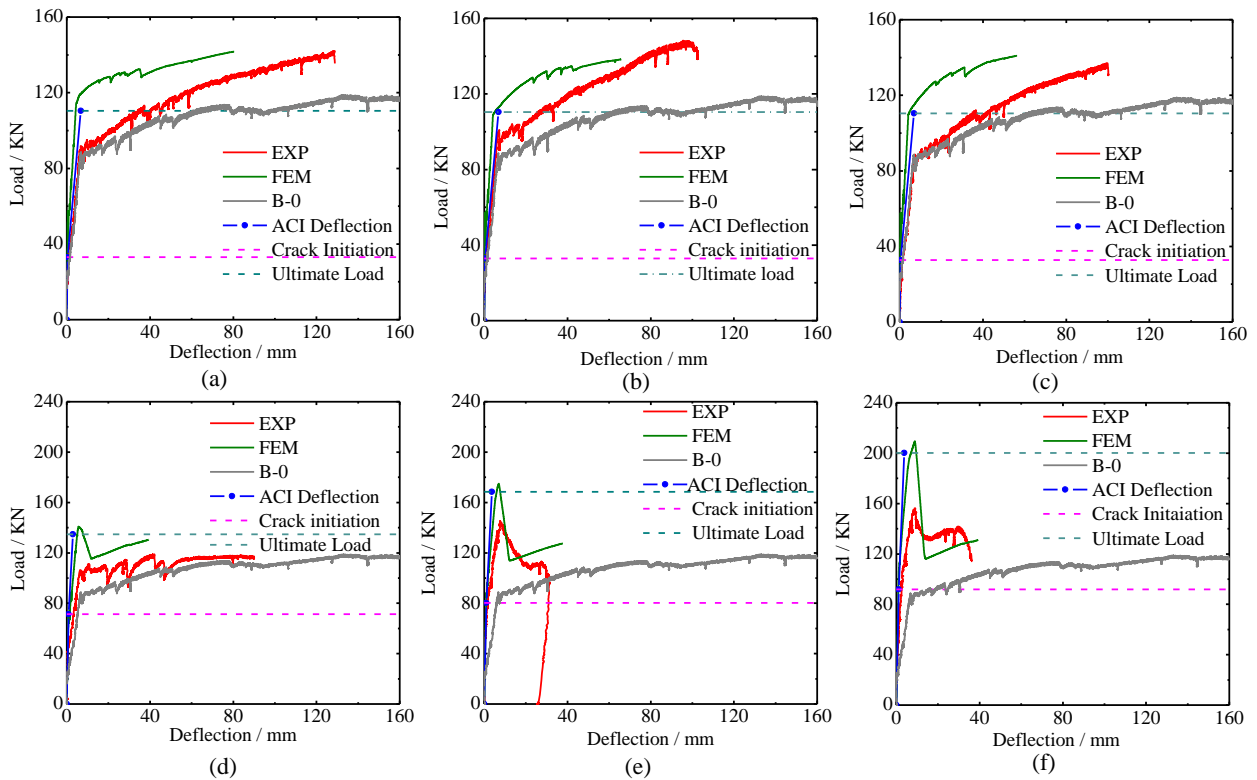


**Fig. 4** Load-deflection behaviors of experiment and FEM analysis for (a) BU-20, (b) BU-40, (c) BU-60, (d) BL-20, (e) BL-40, (f) BL-60 with ACI deflection, ultimate load and crack initiation

presence of micro-cracks. Moreover, the perfect bond between the concrete and steel reinforcement is assumed in the finite element analysis, but the assumption would not be true for the experimental beams. As bond slip occurs, the composite action between concrete and steel reinforcing bar is lost. Therefore, the overall stiffness of the experimental beam is expected to be lower than that of finite element models.

**5.1.1 Top repair series**

**Figs. 4(a) to 4(c)** show the load-deflection curves for the top repair beams for experimental and analytical results along with reference beam (B-0) experimental curve. In top repair beams, the BU-20 specimen shows the same bending behavior as that of the reference beam (B-0) in experimental. After yielding of rebar, experimental and FEM results, indicate that the load increases with a constant gradient up to 142.2KN and 141.76KN in load-deflection relationship respectively. The crushing of UHPFRC repaired beam was observed at 142.2KN, which is 1.2 times more than that of B-0. In BU-40 and BU-60 Specimen, load-displacement relationship and crack condition were the same as that of BU-20. The experimental maximum load of BU-40 was 1.25 times higher compared to B-0. In BU-60, the experiment was terminated earlier because of destruction signs and the maximum load was 137.0KN. The analytical maximum load of BU-60 was 140.96KN. The experimental results are not in good agreement with the analytical results after yielding because of reduction of yielding load due to localized yielding during the experiment as shown in **Figs. 4(a) to 4(c)**. However, the analytical and ACI deflection results are in acceptable agreement.

**5.1.1 Bottom repair series**

**Figs. 4(d) to 4(f)** show the comparison of load-deflection curves for the bottom repair beams for experimental and analytical results with the reference beam (B-0). In general, the flexural capacity of beams with bottom repair increased with the increase of UHPFRC thickness. This is attributed to the

**Table 2** Comparison between experimental and analytical results

Specimen	Ultimate Load (KN)		Cracking Load (KN)		Failure Mode	
	EXP	FEM	FEM	ACI	EXP	FEM
BL-0	118.9	131.86	42.10	33.09	CC	CC
BU-20	142.2	141.76	58.50	33.09	UC	-
BU-40	148.2	138.30	59.25	32.93	R	-
BU-60	137.0	140.96	57.50	32.77	-	-
BL-20	118.9	140.78	78.25	79.24	CC	CC
BL-40	145.3	175.06	86.25	87.99	R	CC
BL-60	156.3	209.40	102.50	99.10	R	CC

CC: concrete crushing, UC: UHPFRC crushing, R: rebar fracture

the high to the high tensile strength and strain hardening of UHPFRC. Thicker UHPFRC layer leads to increase in stiffness before the formation of localized macro-crack. In BL-20 specimen, no increase in flexural capacity was observed compared to reference specimen in the experiment, while analytical and ACI calculation show increase in capacity. This is because localized macro cracks lead to the destruction adhesion between existing concrete and UHPFRC in the experiment. The crack opens with increasing load and crushing of upper edge concrete at the time of load 118.9 KN was observed in the experiment. In BL-40 and BL-60 specimens, the tensile resistance of UHPFRC leads to increase ultimate load 1.22 and 1.31 times reference beam capacity in the experiment while more increase in capacities is observed in analytical and ACI calculations because of tensile properties of UHPFRC are obtained from the tensile tests. Tensile test overestimates the properties and tensile strength reduces for thicker UHPFRC layer because of segregation of fiber. However, an increasing thickness is advantageous, since it leads to smaller deformations for a given load and formation of

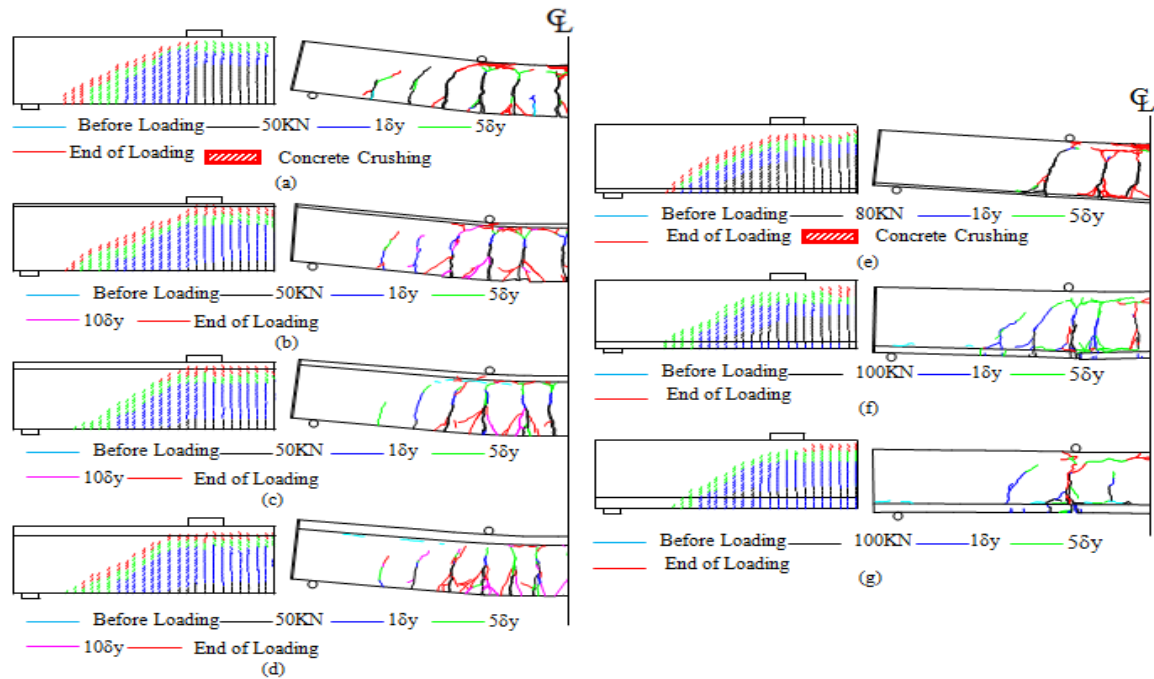


Fig. 5 Crack patterns of experiment and FEM analysis for (a) B-0, (b) BU-20, (c) BU-40, (d) BU-60, (e) BL-20, (f) BL-40, (g) BL-60

of localized macro-cracks at higher load under service conditions, thus, improving durability of concrete member.

### 5.2 Loads at cracking

Table 2 shows the cracking load, ultimate load and failure mode of the specimens by loading test and analytical results. The comparison of the analytical cracking load for lower repair beams shows acceptable agreement with ACI cracking load. The cracking load increases with the increase of UHPFRC thickness because thicker UHPFRC layer leads to an increase of the height of Whitney stress block, thus, delaying the formation of localized macro-cracks results in improving the protection function under service conditions. The analytical cracking load of the reference beams is 21.4% higher than ACI calculations. This is possibly due to the relative homogeneity of the finite element models when compared to the relative heterogeneity of the experimental beams that contain a number of micro-cracks. The analytical cracking load of the top repair beams are not in close agreement with the ACI cracking load. Moreover, the analytical cracking load is not increased significantly with the increase in UHPFRC thickness because the UHPFRC is in the compression zone. The failure modes of the specimens were different in experiment and analysis because localized macro-cracks lead to fracture of rebar during experiments. The fracture of rebar is not observed in the analysis due to high assumed value of the strain at the maximum tensile strength of rebar  $\epsilon_{su} = 24\%$ . The concrete crushing was observed in analytical results. The failure modes of the top repair beams were not observed because of the convergence failure in the analysis.

### 5.3 Crack patterns

Fig. 5 shows the comparison of analytical and experimental cracks. The comparison reveals that experimental crack patterns have few macro-cracks observed visually while the analytical crack patterns have many cracks at regular spacing. First vertical cracks are formed in constant moment region. The cracks propagate upwards as the loading increases. In top repair beams, the neutral axis moves to the top surface with the progress of cracking. The diagonal cracks start to form

before the failure of beams in the shear span. In bottom repair beams, first vertical cracks in ordinary concrete are formed in constant moment region. The cracks propagate to UHPFRC layer as the loading increases. The cracks propagated perpendicular to the UHPFRC layer. The cracking loading increases in case of bottom repair beam because of the high tensile strength of UHPFRC. The analytical cracks show good agreement with experiment and the same pattern is observed.

## 6. CONCLUSIONS

In this study, the existing concrete structure is intended to repair with UHPFRC as cross-sectional restorative material. The results show that the use of UHPFRC in structural elements made of cementitious materials leads to higher stiffness and to an increased bending capacity compared to the previously repaired thickness. Moreover, the UHPFRC significantly delay the crack formation under service conditions, thus guaranteeing the protection function i.e. durability. In future based on the results of this study and additional experiments, the structural performance of UHPFRC as a strengthening material can be utilized.

## REFERENCES

- 1) Brühwiler, E and Denarie E.: Rehabilitation and strengthening of concrete structures using ultra-high performance fiber reinforced concrete, Concrete Repair, Rehabilitation and Retrofitting- III, pp.72-79, 2012.
- 2) Rossi, P.: Development of new cement composite material for construction, Proc., Innovations and Developments in Concrete Materials and construction, Dundee, Scotland, 17-9, 2002.
- 3) Habel, K.: Structural behavior of elements combining ultra-high performance fiber reinforced concrete and reinforced concrete, Doctoral thesis No. 3036, 2004.
- 4) O. Buyukztruk.: Nonlinear analysis of reinforced concrete structures, Vol. 7, PP. 149-156, 1977.
- 5) H. Matsuda et al.: Ultimate behavior of RC beams with PIC boards in flexural compression zone, Department of Structural Engineering, Nagasaki University, Japan.